DOI: 10.1002/ejic.200800799

The Effect of Steric Crowding on Porphyrin Conformation and Ring Orientations in a Series of Iron(III) μ-Oxo Dimers Containing *meso*-Nitrooctaethylporphyrins

Ranjan Patra,[a] Susovan Bhowmik,[a] Sudip Kumar Ghosh,[a] and Sankar Prasad Rath*[a]

Keywords: Iron / Porphyrinoids / Structure–activity relationships / Structure elucidation

We have examined the electronic and geometrical effects of the progressive addition of bulky electron-withdrawing NO_2 groups at the adjacent *meso* positions of Fe^{III}-μ-oxo octaethylporphyrin dimers. The successive addition of mono-, di-, tri-, and tetranitro substituents at the *meso* positions increases the steric congestion at the periphery, which leads to distortion of the porphyrin macrocycle. The X-ray structures of four such molecules $[Fe(din\text{-}OEP)]_2O$, $[Fe(trn\text{-}OEP)]_2O$, $[Fe(tn\text{-}OEP)]_2O$ (triclinic), and $[Fe(tn\text{-}OEP)]_2O$ (monoclinic) have been determined; $[Fe(tn\text{-}OEP)]_2O$ authenticates the first structurally characterized oxo-bridged dimer with a dodecasubstituted and most-distorted porphyrin reported so far and also shows a significant increase in the $Fe–N_p$ and Fe–O distances and the displacement of Fe from mean porphyrin plane. The most important structural feature of the molecules is the very different torsional angles. As the number of nitro group increases, the torsional angles also increase from $[Fe(OEP)]_2O$ to $[Fe(din\text{-}OEP)]_2O$ and to $[Fe(tn\text{-}OEP)]_2O$. However, in the case of $[Fe(trn\text{-}OEP)]_2O$, the torsional angle is zero, while the angles are very different for both molecules present in the asymmetric unit of $[Fe(tn\text{-}OEP)]_2O$ (triclinic). Our study suggests that ruffling accommodates steric congestion at the periphery and thus reduces inter-ring interactions, which leads to smaller torsional angles. Spectroscopic studies are indicative of strong antiferromagnetic coupling between two high-spin iron(III) centers. The addition of NO_2 groups in the porphyrin macrocycle serves both to protect the reactive *meso* positions from rapid oxidative attack and also to stabilize both porphyrin and metal against any oxidative degradation during catalysis. $[Fe(tn\text{-}OEP)]_2O$ therefore ranks amongst the most-effective catalyst in the oxygenation process.

Introduction

Nonplanar distortions of the porphyrin macrocycle, which results from steric interactions involving the peripheral substituents, have been investigated in order to understand the functional consequences of similar distortions observed in various proteins.[1–4] The conformational variations offer an attractive mechanism for the modulation of a wide range of physical and chemical properties of porphyrins in vitro and in vivo, which has led to the synthesis and structural studies of a large number of sterically crowded porphyrins.[3–5] Knowledge of these inter-relationships may help to better understand the essential parameters that govern the specific action of hemoproteins in biological processes.

Fe^{III}-μ-oxo dimers containing electron-deficient and highly distorted porphyrin macrocycles rank amongst the most-effective catalysts for various oxygenation processes and can be used as biomimetic models for cytochrome P-450.[6–11] It is thus possible that a better understanding of the substituent effects in these compounds might lead to an improved understanding of their structure and reactivity. The environment of the *meso* sites in hemes has been recognized to be sterically constricted.[12] The incorporation of highly electron-withdrawing bulky nitro groups at the *meso* positions of iron(III) octaethylporphyrins induces substantial steric crowding at the periphery, which leads to macrocycle deformations, and the rings becomes considerably electron deficient. In the present work, we have examined the structural and electronic effects of the progressive addition of bulky NO_2 groups at the adjacent *meso* carbon positions of the Fe^{III}-μ-oxo octaethylporphyrin dimer and scrutinized their effects on macrocycle conformation and inter-ring orientation, which results in torsional angles ($N_p–Fe–Fe'–N'_p$ dihedral angle). Previous theoretical and experimental studies have shown that the near-eclipsed orientation (torsional angle of 17–23°) of the two octaethylporphyrinato cores is primarily the result of interdigitation of the ethyl groups in all derivatives with only ethyl groups at the periphery, while *meso*-substituted derivatives show a nearly staggered orientation (torsional angle of ca. 45°) in order to minimize the intra- and inter-ring interactions.[13] Herein we wish to investigate the effects of both ethyl and *meso*

[a] Department of Chemistry, Indian Institute of Technology Kanpur,
Kanpur-208016, India
E-mail: sprath@iitk.ac.in

Supporting information for this article is available on the WWW under http://www.eurjic.org or from the author.

substitution on the electronic structure and geometry of the oxo-bridged Fe^{III} dimer and examine the consequences of significant steric congestion at the periphery of the macrocycles. Steric congestion also appears to have affected the structure and bond parameters in the core and led to several interesting observations in the series of Fe^{III}-μ-oxo dimers of *meso*-nitrooctaethylporphyrins reported here.

Results and Discussion

Porphyrin macrocycles can be distorted by introduction of sterically demanding substituents at the porphyrin periphery. Successive addition of mono-, di-, tri-, and tetranitro substituents at adjacent *meso* positions of octaethylporphyrins has a marked effect on the structures of the Fe^{III}-μ-oxo dimers. The free ligands 5-mononitrooctaethylporphyrins (mn-H_2OEP), 5,10-dinitrooctaethylporphyrin (din-H_2OEP), and 5,10,15-trinitrooctaethylporphyrins (trn-H_2OEP) were prepared by the reported method of Bonnett and Stephenson,[14] while 5,10,15,20-tetranitrooctaethylporphyrins (tn-H_2OEP) were prepared by the method of Gong and Dolphin.[15] Iron metal is inserted into the cavity by using the standard procedure of Adler and co-workers[16] under nitrogen to form Fe(por)Cl in excellent yields. The dichloromethane solution of Fe(por)Cl was then shaken with 2 N NaOH solution and the solvents evaporated to dryness followed by chromatographic separation in basic alumina with chloroform as eluent to isolate the corresponding Fe^{III}-μ-oxo dimers. Scheme 1 shows the list of all oxo-bridged dimers reported in this paper and their abbreviations. The UV/Vis spectrum of [Fe(mn-OEP)]$_2$O shows the Soret and two Q-bands at 380, 562, and 594 nm, respectively. However, with successive addition of the nitro groups as shown in the series, the Soret band undergoes a blueshift, while the Q bands are all redshifted. The blueshift in the Soret band reflects the extreme close interporphyrin ring separation. For comparison, the Soret band of [Fe(OEP)]$_2$O is observed at 387 nm, while [Fe(OEP)]$_2$-(OH)$^+$ has a strongly blueshifted Soret band at 361.7 nm, which reflects the closeness of the two rings as a result of the hydroxide bridge.[17] Further, for [Fe(tn-OEP)]$_2$O, the Soret band is observed at 369 nm, while a band at 378 nm is observed for monomeric Fe(tn-OEP)Cl.[5b] It is, however, interesting to note that the Soret band slightly shifts to higher wavelengths from [Fe(trn-OEP)]$_2$O (at 361 nm) to [Fe(tn-OEP)]$_2$O because of the presence of highly deformed porphyrin cores in the latter, which restricts the cores from coming too close. All the complexes have been isolated in the solid state in good yields and are structurally characterized with the exception of [Fe(mn-OEP)]$_2$O, in which single crystals suitable for X-ray crystallography could not be obtained (Scheme 1).

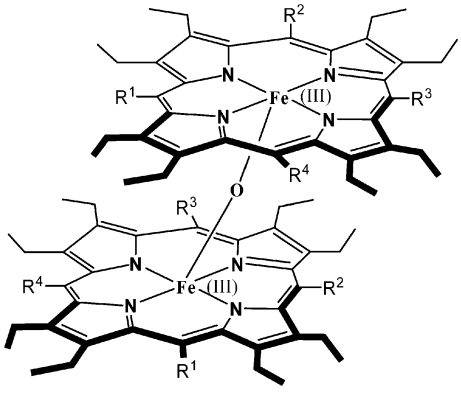

R^1	R^2	R^3	R^4	Complex
NO_2	H	H	H	[Fe(mn-OEP)]$_2$O
NO_2	NO_2	H	H	[Fe(din-OEP)]$_2$O
NO_2	NO_2	NO_2	H	[Fe(trn-OEP)]$_2$O
NO_2	NO_2	NO_2	NO_2	[Fe(tn-OEP)]$_2$O

Scheme 1.

Crystallographic Characterization of [Fe(din-OEP)]$_2$O

Slow diffusion of acetonitrile into a dichloromethane solution of [Fe(din-OEP)]$_2$O at room temperature gave dark brown crystals from which an appropriate crystal was chosen for X-ray diffraction experiments. [Fe(din-OEP)]$_2$O crystallizes in the monoclinic crystal system with the space group $P2(1)/n$, and one full molecule of the complex and one acetonitrile solvent molecule are present in the asymmetric unit. Two perspective views of the molecule are shown in Figure 1, and selected bond lengths and angles

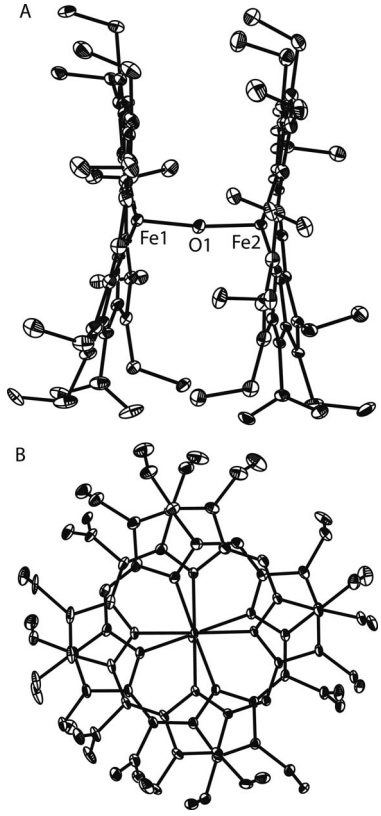

Figure 1. Two perspective views [A, side view; B, top view] of [Fe(din-OEP)]$_2$O showing 50% thermal contours for all non-hydrogen atoms.

are given in Table 1. As seen, Fe–N_p distances, which are the in-plane distances to the porphyrin nitrogen atoms, are in the narrow range of 2.076 to 2.100 Å, the Fe–O distances are 1.755(3) and 1.757(3) Å, and the Fe–O–Fe angle is 172.6(2)°. Moreover, the Fe^{III} centers are displaced by 0.57 and 0.52A° from the mean porphyrin plane (24 atoms) for both the cores towards the oxo oxygen atom. These values are normal for any high-spin Fe^{III}-μ-oxo porphyrin dimers reported in the literature.[11a,13,18,19]

Table 1. Selected bond lengths [Å] and angles [°].

Bond lengths [Å]	[Fe(din-OEP)]$_2$O		[Fe(trn-OEP)]$_2$O
Fe1–N1	2.086(4)		2.079(3)
Fe1–N2	2.096(4)		2.094(3)
Fe1–N3	2.084(4)		2.084(3)
Fe1–N4	2.080(4)		2.083(3)
Fe2–N1		2.082(4)	
Fe2–N2		2.100(4)	
Fe2–N3		2.089(4)	
Fe2–N4		2.076(4)	
Fe1–O1	1.755(3)		1.7576(9)
Fe2–O1		1.757(3)	
Bond angles [°]			
N1–Fe1–N2	86.75(16)		86.63(12)
N1–Fe1–N3	150.71(16)		155.05(11)
N1–Fe1–N4	87.39(16)		88.03(12)
N2–Fe1–N3	86.78(15)		87.63(12)
N2–Fe1–N4	155.97(16)		154.44(11)
N3–Fe1–N4	87.02(14)		86.75(11)
N1–Fe2–N2		87.54(15)	
N1–Fe2–N3		150.21(16)	
N1–Fe2–N4		86.30(17)	
N2–Fe2–N3		86.49(15)	
N2–Fe2–N4		156.39(16)	
N3–Fe2–N4		87.61(16)	
N1–Fe1–O1	104.60(17)		101.44(8)
N2–Fe1–O1	100.03(14)		103.42(8)
N3–Fe1–O1	104.65(15)		103.51(8)
N4–Fe1–O1	104.00(16)		102.14(8)
N1–Fe2–O1		105.28(15)	
N2–Fe2–O1		100.27(15)	
N3–Fe2–O1		104.50(15)	
N4–Fe2–O1		103.33(17)	
Fe1–O1–Fe2	172.6(2)		180.00(3)

As seen in Figure 1, two nitro groups are placed in the *cisoid meso* position in each core and have positional disorder in one of the two porphyrin cores. One nitro group in core 1 is distributed at the two *meso* sites (at C5 and C20) with three fractional occupancies. There are also orientation disorders for some of the ethyl substituents. The relative orientations of the two porphyrin rings make an average N_p–Fe–Fe′–N'_p dihedral angle (torsional angle) of 18.8°, while the interplanar angle is only 4.3°.

However, the Fe^{III}-μ-oxo dimer containing *trans*-5,15-dinitrooctaethylporphyrin, which is also structurally known from before, shows an eclipsed ring orientation [torsional angle of 1.1(20)°], while the nitro groups are staggered by 90° from one residue to the other.[11a] The average Fe–N_p distance of 2.090(7) Å is found, while the Fe–O distances are 1.763(4) and 1.751(4) Å. The two porphyrin cores in the molecule are not parallel, which makes the Fe–O–Fe angle considerably less, 167.9(3)°. The Fe atoms are displaced from the porphyrin plane towards the bridging oxo oxygen atom by 0.46 (core 1) and 0.49 Å (core 2).

Crystallographic Characterization of [Fe(trn-OEP)]$_2$O

Dark brown crystals of [Fe(trn-OEP)]$_2$O were grown by slow diffusion of methanol into a chloroform solution of [Fe(trn-OEP)]$_2$O at room temperature. The complex crystallizes in the triclinic crystal system with the space group $P\bar{1}$, with one-half of the molecule present in the asymmetric unit, and the bridging oxo oxygen atom is located at the center of inversion. Two perspective views of the molecule are shown in Figure 2, and selected bond lengths and angles are given in Table 1. The Fe^{III} center is displaced by 0.48A° from the mean porphyrin plane (24 atoms) towards the oxo oxygen atom and forms a linear Fe–O–Fe bond [180.00(3)°]. The Fe–N_p distances are in the narrow range of 2.079 to 2.094 Å, while the Fe–O distance is 1.7576(9) Å. These distance and angles are normal for any Fe^{III}-μ-oxo porphyrin dimers reported in the literature.[11a,13,18,19] However, there is no disorder in the positions of the *meso* nitro groups as well as in the ethyl group orientations. The two rings are

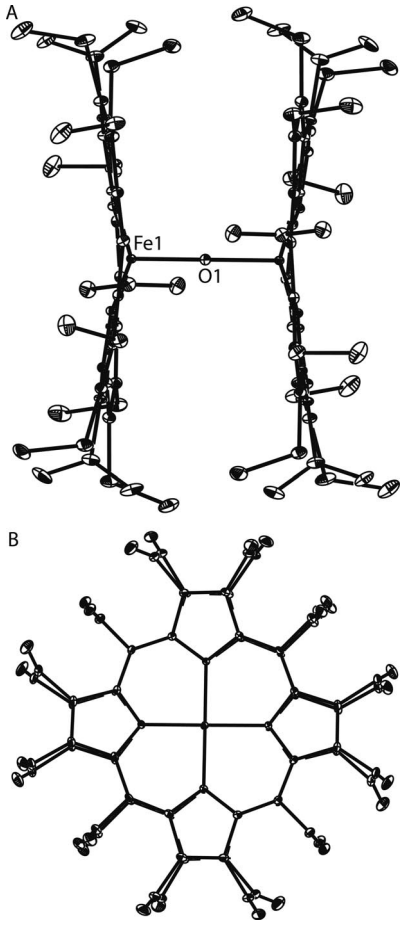

Figure 2. Two perspective views [A, side view; B, top view] of [Fe(trn-OEP)]$_2$O showing 35% thermal contours for all non-hydrogen atoms.

perfectly parallel with a 4.48 Å interplanar separation and the orientation of the rings is fully eclipsed. This is the first example of fully eclipsed ring orientation for a Fe^{III}-μ-oxo dimer reported so far.

Crystallographic Characterization of $[Fe(tn\text{-}OEP)]_2O$

Dark brown crystals were grown by slow diffusion of acetonitrile into tetrahydrofuran solution of $[Fe(tn\text{-}OEP)]_2O$ at room temperature. The molecule crystallizes in the triclinic crystal system with the space group $P\bar{1}$ and two independent molecules in the asymmetric unit. Two perspective views of molecule 1 and molecule 2 are shown in Figures 3 and 4, respectively. Selected bond lengths and angles are given in Table 2. However, only one nitro group in core 1 (molecule 1) is disordered and has been distributed over two different orientations, and there is disorder in some of the ethyl groups. However, the two porphyrin rings in each molecule make an average N_p–Fe–Fe′–N'_p dihedral angle (torsional angle) of 24.3° (molecule 1) and 15.7° (molecule 2), while the interplanar angles are 2.1° and 2.8°, respectively. Moreover, the two rings in each molecule are so close to each other that about half of the oxygen atom from the nitro groups and methylene carbon atoms of the adjacent peripheral ethyl groups are close to the van der Waals contacts of the atoms. The closest intramolecular O···C nonbonding distances are 3.135 Å and 3.076 Å for molecules 1 and 2, respectively, which are well below the van der Waals radii of the atoms. Further, in molecule 1, one nitro group is very close to the other nitro group of the opposite core, and is therefore disordered and distributed with two different folding modes.

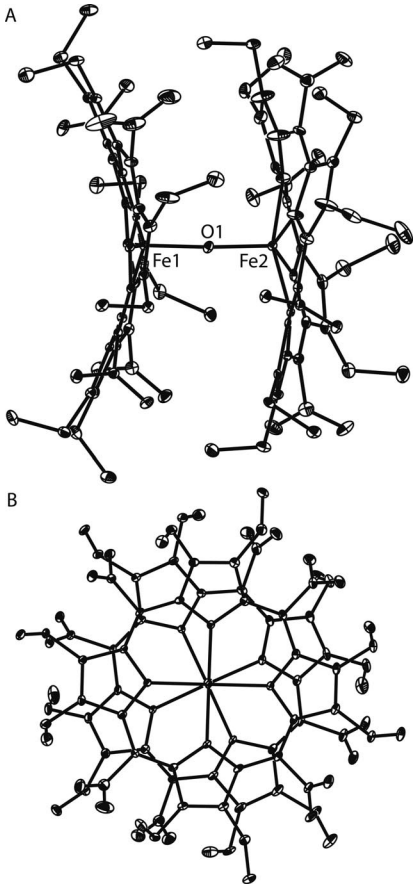

Figure 3. Two perspective views [A, side view; B, top view] of molecule 1 of $[Fe(tn\text{-}OEP)]_2O$ [Tric.] showing 50% thermal contours for all non-hydrogen atoms.

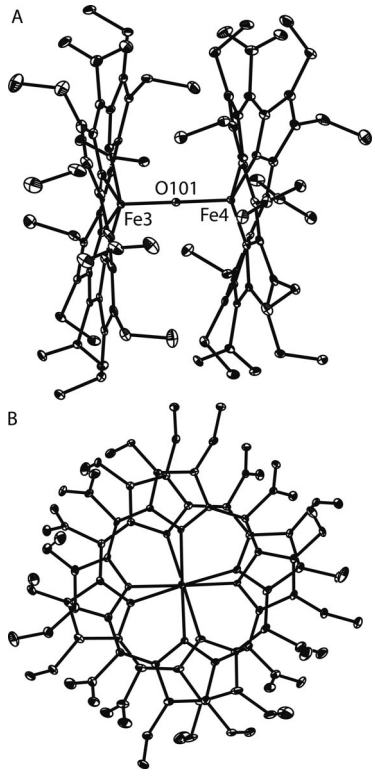

Figure 4. Two perspective views [A, side view; B, top view] of molecule 2 of $[Fe(tn\text{-}OEP)]_2O$ [Tric.] showing 50% thermal contours for all non-hydrogen atoms.

The two independent molecules that are present in the asymmetric unit are similar in their gross core structures but differ in the macrocyclic distortions and bonding parameters. The Fe centers have a five-coordinate square-pyramidal geometry and are displaced towards the oxo oxygen atom by 0.62 (molecule 1) and 0.65A° (molecule 2) from the least-squares plane of the 24 porphyrin atoms. The Fe–N_p distances lie in the narrow range 2.073–2.095 Å for molecule 1 and 2.073–2.114 Å for molecule 2, while the Fe–O distances are 1.769(2) and 1.766(2) Å for molecule 1 and 1.776(2) and 1.775(2) Å for molecule 2. All these distances are substantially longer than corresponding distances in other Fe^{III}-μ-oxo dimers reported here and elsewhere.[13,17,18] The bridging Fe1–O–Fe2 angles are very similar for both molecules, 177.16(17) and 176.64(15)° in molecules 1 and 2, respectively. Further, the interplanar angles between the mean 24-atom planes are 2.1 and 2.8°, respectively, for both the molecules, while the average mean plane separations are 4.77 and 4.88 Å, respectively. One unexpected feature of the molecular structure is that two intramolecular porphyrin rings are oriented in a nearly eclipsed conformation with very different torsional angles (24.3 and

Table 2. Selected bond lengths [Å] and angles [°].

Bond lengths [Å]	[Fe(tn-OEP)]$_2$O [Tric.] molecule 1		[Fe(tn-OEP)]$_2$O [Tric.] molecule 2		[Fe(tn-OEP)]$_2$O [Mono.]	
Fe1–N1	2.073(3)		2.083(3)		2.100(3)	
Fe1–N2	2.093(3)		2.109(3)		2.082(3)	
Fe1–N3	2.080(3)		2.073(3)		2.114(3)	
Fe1–N4	2.089(3)		2.114(3)		2.082(3)	
Fe2–N1		2.085(3)		2.085(3)		2.108(3)
Fe2–N2		2.095(3)		2.081(3)		2.088(3)
Fe2–N3		2.083(3)		2.106(3)		2.102(3)
Fe2–N4		2.089(3)		2.076(3)		2.092(3)
Fe1–O1	1.769(2)		1.776(2)		1.771(2)	
Fe2–O1		1.766(2)		1.775(2)		1.772(2)
Bond angles [°]						
N1–Fe1–N2	86.78(12)		86.14(12)		86.55(12)	
N1–Fe1–N3	157.79(12)		155.35(12)		145.21(11)	
N1–Fe1–N4	87.01(12)		86.75(11)		86.14(12)	
N2–Fe1–N3	87.26(11)		86.60(12)		86.30(11)	
N2–Fe1–N4	146.34(13)		146.17(12)		155.15(12)	
N3–Fe1–N4	86.17(12)		86.26(11)		86.26(11)	
N1–Fe2–N2		87.12(11)		86.15(11)		86.02(11)
N1–Fe2–N3		145.88(12)		142.94(11)		144.06(11)
N1–Fe2–N4		86.22(11)		85.87(11)		85.94(11)
N2–Fe2–N3		85.93(12)		85.74(11)		85.91(11)
N2–Fe2–N4		156.48(11)		154.71(12)		155.00(11)
N3–Fe2–N4		87.02(11)		86.27(11)		86.82(11)
N1–Fe1–O1	99.60(12)		104.94(11)		105.37(11)	
N2–Fe1–O1	106.37(11)		103.75(11)		101.48(11)	
N3–Fe1–O1	102.60(11)		99.67(11)		109.42(11)	
N4–Fe1–O1	107.28(13)		110.04(11)		103.35(11)	
N1–Fe2–O1		108.47(12)		106.26(11)		109.27(11)
N2–Fe2–O1		102.60(11)		106.33(11)		101.03(11)
N3–Fe2–O1		105.65(12)		110.73(11)		106.64(11)
N4–Fe2–O1		100.91(11)		98.94(11)		103.96(10)
Fe1–O1–Fe2	177.16(17)		176.64(15)		175.08(14)	

15.7° for molecules 1 and 2, respectively), although the relative ("inward"/"outward") orientation of the ethyl groups within the molecule are exactly the same for both molecules. Therefore, interdigitation of the peripheral ethyl groups is not responsible for the difference in the torsional angles. The packing of [Fe(tn-OEP)]$_2$O molecules in the unit cell is illustrated in Figure 5, and, as can be seen, there are also no unusually short intermolecular contacts in the crystal packing of the molecules.

Another isostructural form of [Fe(tn-OEP)]$_2$O crystallizes in the monoclinic $P2(1)/n$ space group; the crystal was grown by slow diffusion of cyclohexane into the chloroform/1% ethanol solution of [Fe(tn-OEP)]$_2$O. One full molecule and a few disordered solvent molecules are present in the asymmetric unit, and selected bond lengths and angles are given in Table 2. The structures of [Fe(tn-OEP)]$_2$O in the two different crystalline forms (triclinic and monoclinic) are quite similar in all important aspects. In the monoclinic form, the Fe–N_p distances are in the narrow range 2.082(3)–2.114(3) Å, while the Fe–O distances are 1.771(2) and 1.772(2) Å and the Fe–O–Fe angle is 175.08(14)°. The Fe^{III} center is displaced by 0.66A° towards the oxo oxygen atom from the mean porphyrin plane (24 atoms). There is also no disorder in the position of the *meso* nitro groups as well as in the ethyl group orientation. The relative orientation of the two rings in the molecule are such that torsional angle of 24.2° forms (average N_p–Fe–Fe′–N′$_p$ dihedral angles) with an interplanar angle of 3.7°.

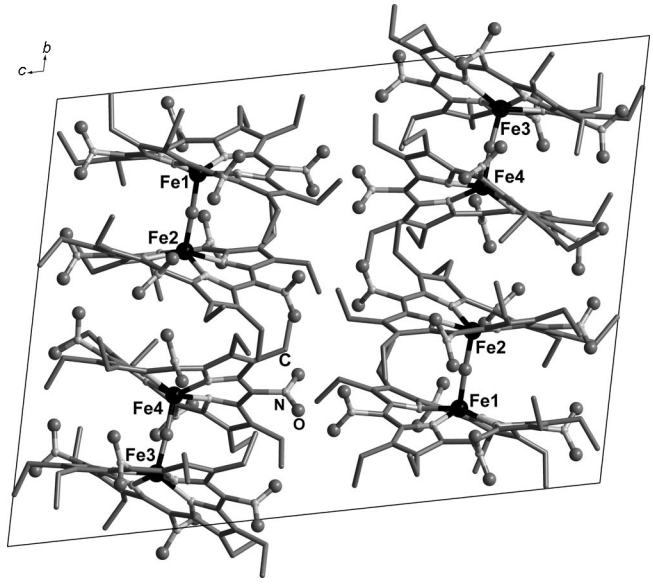

Figure 5. Diagram illustrating the packing of [Fe(tn-OEP)]$_2$O [Tric.] molecules in the unit cell.

Table 3. Selected geometrical parameters.[a]

Complex	Fe–N_p[b]	Fe–O[b]	Fe–O–Fe[c]	Fe···Fe[b]	MPS[b,d]	ΔC_m[e]	ΔC_β[e]	Δ_{24}[f]	Δ_{24}^{Fe}[g]	Φ[h]
$[Fe(OEP)]_2O$ [Tric.][i]	2.076(3)	1.758(3)	172.2(2)	3.50	4.50	0.03	0.10	0.05	0.49	17.0
	2.078(3)	1.754(3)				0.04	0.13	0.07	0.51	
$[Fe(OEP)]_2O$ [Mono][i]	2.082(4)	1.762(4)	176.2(2)	3.50	4.60	0.04	0.13	0.04	0.56	16.8
	2.078(4)	1.748(4)				0.03	0.05	0.02	0.52	
$[Fe(din\text{-}OEP)]_2O$	2.086(4)	1.755(3)	172.6(2)	3.50	4.58	0.08	0.35	0.17	0.57	18.8
	2.086(4)	1.757(3)				0.07	0.35	0.19	0.52	
$[Fe(trn\text{-}OEP)]_2O$	2.085(3)	1.7576(9)	180	3.51	4.48	0.23	0.11	0.12	0.48	0.0
$[Fe(tn\text{-}OEP)]_2O$ [Mono.]	2.095(3)	1.771(2)	175.08(14)	3.54	4.87	0.10	0.72	0.36	0.64	24.2
	2.096(3)	1.772(2)				0.12	0.78	0.40	0.69	
$[Fe(tn\text{-}OEP)]_2O$ [Tric.] molecule 1	2.084(3)	1.769(2)	177.16(17)	3.53	4.77	0.09	0.77	0.39	0.61	24.3
	2.088(3)	1.766(2)				0.20	0.71	0.38	0.63	
$[Fe(tn\text{-}OEP)]_2O$ [Tric.] molecule 2	2.095(3)	1.776(2)	176.64(15)	3.55	4.88	0.24	0.57	0.32	0.61	15.7
	2.087(3)	1.775(2)				0.28	0.82	0.45	0.70	

[a] Two lines are for cores 1 and 2, respectively. [b] Average value in Å. [c] Value in °. [d] Distance between two least squares planes (24 atoms). [e] Average displacement (in Å) from four porphyrin nitrogen atoms. [f] Average displacement (in Å) of the 24 atoms from the least-squares plane of the porphyrin. [g] Displacement (in Å) of iron from the least-squares plane of the porphyrin (24 atoms). [h] Average of the N_p–Fe–Fe′–N'_p dihedral angle. [i] Taken from ref.[13]

The present study shows that the addition of bulky and strong electron-withdrawing nitro groups at the *meso* positions have a significant impact on the electronic and structural properties of metalloporphyrins. The successive addition of mono-, di-, tri-, and tetranitro substituents at adjacent *meso* positions of the iron octaethylporphyrins increases the steric congestion at the periphery of the molecules, which leads to distortions of the porphyrin macrocycle. As a result, the average deviation of the 24 macrocycle atoms increases with increasing *meso* substitution, with a lone exception in the case of trinitro-substituted porphyrins. However, the effect is magnified for the case of the tetranitro-substituted complex $[Fe(tn\text{-}OEP)]_2O$. Table 3 presents a comparison of the structures and geometrical features of all complexes reported here. The Fe atoms are displaced from the mean porphyrin plane towards the oxo oxygen atom in all cases; however, the extent of displacement increases with increasing ring distortion. The presence of four electron-withdrawing bulky nitro groups at the *meso* position causes significant distortion of the porphyrin macrocycle and provides an interesting modulation of the macrocycle properties, which leads to a significant increase in the average Fe–N_p and Fe–O distances and in the metal···metal and mean porphyrin plane separations, as seen in Table 3.

The porphyrin rings are distorted in all complexes reported here; among them, the tetranitro-substituted cores are distorted the most. This is best illustrated in Figure 6, where the out-of-plane displacement (in units of 0.01 Å) of the core atoms is compared. The nomenclature that describes the types of distortions commonly observed in nonplanar porphyrins was originally suggested by Scheidt and Lee.[20] In a saddle conformation, alternate pyrrole rings tilt up and down with respect to the mean porphyrin plane (24 atoms) and the *meso* carbon atoms lie on the least-squares plane. In a ruffle conformation, alternate pyrrole rings twist clockwise or counterclockwise about the metal–nitrogen bond and the *meso* carbon atoms move alternately above or below the least-squares plane of the 24-atom porphyrin core. As is evident from Figure 6, the ring distortions for $[Fe(din\text{-}OEP)]_2O$ and $[Fe(tn\text{-}OEP)]_2O$ can be described as saddle-type with alternating displacement of the pyrrole rings below and above the mean porphyrin plane, while the pyrrole nitrogen and *meso* carbon atoms lie on the plane. However, for $[Fe(trn\text{-}OEP)]_2O$, the rings are mostly distorted in a ruffle-type fashion and are more planar relative to other rings. The average out-of-plane displacement of the 24 atoms of the porphyrin core increase in the order $[Fe(trn\text{-}OEP)]_2O < [Fe(din\text{-}OEP)]_2 < [Fe(tn\text{-}OEP)]_2O$.

Shelnutt et al. has developed the normal-coordinate structural decomposition method (NSD),[21,22] which simulates any porphyrin distortion by linear combinations of six normal deformations that include, in addition to saddle (sad) and ruffle (ruf) distortions, dome (dom), wave [wav(x) and wav(y)], and propeller (pro) conformations and total out-of plane displacements (Doop).[21,22] The results of NSD analysis of the complexes are presented in Table 4. The total distortion (Doop) increases in the order $[Fe(trn\text{-}OEP)]_2O < [Fe(din\text{-}OEP)]_2 < [Fe(tn\text{-}OEP)]_2O$. The porphyrin rings are mostly distorted in a saddle-type fashion for $[Fe(din\text{-}OEP)]_2O$ and $[Fe(tn\text{-}OEP)]_2O$, while the ring distortions are mostly ruffle-type in $[Fe(trn\text{-}OEP)]_2O$. Moreover, a significant increase in ruffling is observed for the rings in molecule 2 relative to molecule 1. However, all the cores also have a small but significant amount of dome contribution.

Table 5 shows all structurally characterized Fe^{III}-μ-oxo porphyrin dimers that have distorted porphyrin macrocycles; our complex $[Fe(tn\text{-}OEP)]_2O$ has the most-distorted macrocycle with a significant increase in the average Fe–N_p and Fe–O distances and Fe displacements from the mean porphyrin plane. Moreover, the complex represents first Fe^{III}-μ-oxo dimer with a dodeca-substituted porphyrin macrocycle. In contrast, the Fe–N_p distances generally decrease with increasing nonplanarity of the porphyrin macrocycle.[1–5] However, the porphyrin cores in $[Fe(tn\text{-}OEP)]_2O$ are highly distorted in a saddle-type fashion. In contrast, highly saddle-distorted complexes are known[7a] to

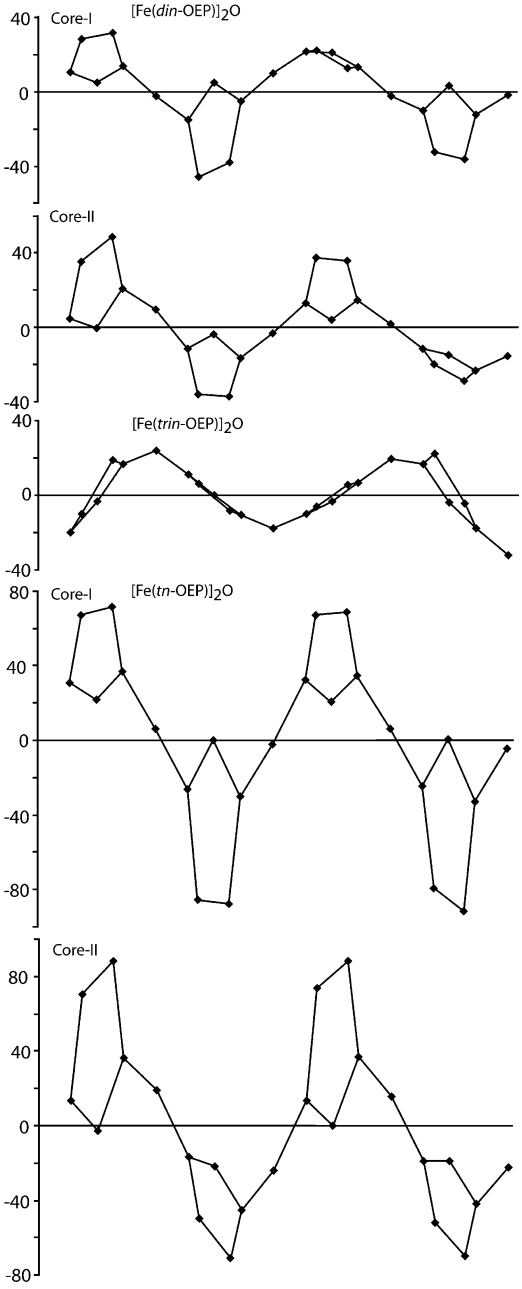

Figure 6. Diagrams comparing the out-of-plane displacement (units of 0.01 Å) of the porphyrin core atoms from the mean porphyrin plane for $[Fe(din\text{-}OEP)]_2O$, $[Fe(trn\text{-}OEP)]_2O$, and $[Fe(tn\text{-}OEP)]_2O$ [molecule 1, triclinic].

favor monomeric porphyrin complexes because of severe steric clash between the substituents in the two adjacent porphyrin cores.

The factors that affect the torsional angles can now be discussed. Previous theoretical and experimental studies have shown that the near-eclipsed orientation (torsional angle of 17–23°) of the two octaethylporphyrinato cores is primarily the result of interdigitation of ethyl groups in all derivatives with only ethyl groups at the periphery, while *meso*-substituted derivatives show an almost-staggered orientation (torsional angle ca. 45°) in order to minimize the intra- and inter-ring interactions.[13] In the present work, as the number of nitro groups increase in the *meso* positions, the torsional angles also increase from $[Fe(OEP)]_2O$ (≈17°), to $[Fe(din\text{-}OEP)]_2O$ (≈18.8°), and to $[Fe(tn\text{-}OEP)]_2O$ (≈24°) (Table 3). This feature and the pronounced nonplanarity of the cores results from the increasing significant congestion at the periphery. However, the extent of increase in the torsional angles is smaller in the series, since the steric congestion also appears to affect the structure and bond parameters in the core, which may contribute to a decreasing of the torsional angles. For $[Fe(trn\text{-}OEP)]_2O$, the two rings are fully eclipsed, in spite of the three bulky nitro groups at the *cisoid meso* positions. Tables 3 and 5 show that both $[Fe(din\text{-}OEP)]_2O$ and $[Fe(trn\text{-}OEP)]_2O$ have very similar Fe–N_p and Fe–O distances, with the exception of inter-ring interactions, which would be expected to be somewhat smaller for $[Fe(trn\text{-}OEP)]_2O$ because of the linear Fe–O–Fe bond and also because of parallel porphyrin ring orientations. However, the rings in $[Fe(trn\text{-}OEP)]_2O$ are distorted in a ruffle-type fashion and are more planar; all three nitro groups are placed at opposite faces of the two rings, which leads to a fully eclipsed ring orientation in order to minimize the intra- and inter-ring interactions. The ruffling deformation of the core accommodates the steric congestion of the peripheral substituents.[18g] Small torsional angles are also observed in the case of $[Fe(ODM)]_2O$[18g] (3.84°) and $[Fe(5,15\text{-dinitro OEP})]_2O$[11a] [1.1(20)°]. Ruffling core deformations and the positioning of the substituents at *trans* positions to minimize the intra- and inter-ring interactions are the most probable cause for the very small torsional angles in all these cases.

For $[Fe(tn\text{-}OEP)]_2O$, the observed torsional angles are much smaller than that expected for the almost staggered orientation (torsional angle of ca. 45°) of Fe^{III}-oxo-bridged

Table 4. Normal-coordinate structural decomposition (NSD) analysis of the complexes.[a]

Complex	Doop	B_{2u}, saddle	B_{1u}, ruffle	A_{2u}, dome	$E_g(x)$, wave(x)	$E_g(y)$, wave(y)	A_{1u}, propeller	sum	ruf/sum [%]
$[Fe(din\text{-}OEP)]_2O$	1.0254	–0.9563	0.0874	0.2748	–0.1235	–0.1962	–0.0013	1.6395	5.3
	1.1272	1.0751	0.2073	–0.1511	–0.0810	0.2056	–0.0082	1.7283	12.0
$[Fe(trn\text{-}OEP)]_2O$	0.7149	–0.0334	0.6761	–0.1022	–0.0982	0.1810	0.0061	1.097	61.6
$[Fe(tn\text{-}OEP)]_2O$ [Tric.] molecule 1	2.3887	2.3604	–0.1377	0.3357	–0.0359	–0.0215	–0.0324	2.9236	4.7
	2.2571	–2.1483	–0.5877	0.3633	0.0298	–0.0018	–0.0313	3.1622	18.6
$[Fe(tn\text{-}OEP)]_2O$ [Tric.] molecule 2	1.9046	–1.7419	0.7079	–0.2538	0.1512	–0.0507	–0.0486	2.9541	24.0
	2.6602	–2.5054	–0.7828	–0.4265	0.0378	0.0520	0.0280	3.8325	20.4
$[Fe(tn\text{-}OEP)]_2O$ [Mono.]	2.2431	2.2071	–0.1897	–0.3439	0.0553	0.0515	–0.0181	2.8656	6.6
	2.4497	–2.3963	–0.0274	0.4570	0.0579	–0.2105	–0.0383	3.1874	0.9

[a] Two lines are for cores 1 and 2, respectively.

Table 5. Fe^{III}-μ-oxo porphyrin dimers with distorted porphyrin macrocycles.

Complex	Fe–N_p[a]	Fe–O[a]	Fe–O–Fe[b]	Δ^{Fe}_{24}[c]	Δ_{24}[d]	ΔC_β[e]	ΔC_m[e]	Φ[f]	MPS[g]	Ref.
$[TPPBr_4Fe]_2O$	2.081(9)	1.758(8)	177.9(5)	0.54	0.34	0.62	0.35	28.0	4.58	[18d]
$[TPPBr_4Fe]_2O$	2.070(3)	1.7583(4)	178.7(2)	0.53	0.33	0.61	0.30	34.2	4.57	[18a]
$[Fe(TPC)]_2O$	2.084(7)	1.755(11)	180	0.55	0.21	0.34	0.26	30.2	4.60	[18f]
$[Fe(ODM)]_2O$	2.065(4)	1.752(1)	178.5(6)	0.53	0.26	0.18	0.54	3.8	4.55	[18g]
$[Fe(TTP)]_2O$	2.086(12)	1.74(3)	178.2(3)	0.52	0.11	0.17	0.07	30.5	4.51	[18b]
$[Fe(PCTPP)]_2O$	2.08(2)	1.743(3)	180	0.53	0.21	0.32	0.25	29.2	4.54	[18c]
$[(NMeTPP)Fe–O–Fe(TPP)]ClO_4$	2.066(6)	1.740(4)	165.4(3)	0.46	0.23	0.45	0.17	30.2	4.40	[18e]
$[Fe(din\text{-}OEP)]_2O$	2.086(4)	1.756(3)	172.6(2)	0.54	0.18	0.35	0.08	18.8	4.58	this work
$[Fe(trn\text{-}OEP)]_2O$	2.085(3)	1.7576(9)	180	0.48	0.12	0.11	0.23	0.0	4.48	this work
$[Fe(tn\text{-}OEP)]_2$ [Tric.][h]	2.086(3)	1.767(2)	177.2(2)	0.62	0.38	0.74	0.14	24.3	4.77	this work
	2.091(3)	1.775(2)	176.6(1)	0.65	0.39	0.69	0.26	15.7	4.88	
$[Fe(tn\text{-}OEP)]_2O$ [Mono.]	2.095(3)	1.771(2)	175.1(1)	0.66	0.38	0.75	0.11	24.2	4.87	this work

[a] Average value in Å. [b] Value in [°]. [c] Displacement (in Å) of iron from least-squares plane of the porphyrin (24 atoms). [d] Average displacement (in Å) of the 24 atoms from the least-squares plane of the porphyrin. [e] Average displacement (in Å) from four porphyrin nitrogen atoms. [f] Average value of N_p–Fe–Fe′–N′$_p$ dihedral angles. [g] Distance between two least-squares planes (24 atoms). [h] Two lines are for molecules 1 and 2, respectively.

dimers of *meso*-substituted porphyrins. For example, the torsional angles observed for most of the Fe^{III}-μ-oxo dimers containing tetraarylporphyrins are 30–35°.[18e,18f,19c,19e,19g] The relatively large torsional angle is surely the result of minimizing interactions between the bulky peripheral aryl groups at the *meso* positions. In $[Fe(TF_5PP)]_2O$, the peripheral groups in the *meso* positions are even bulkier pentafluorophenyl substituents, and as a result, the torsional angle increases to 43°, close to the maximum value of 45°.[19d] However, as can be seen from Table 5, the mean plane separation and extent of ring deformations are highest in the case of $[Fe(tn\text{-}OEP)]_2O$, in which the steric repulsions between the rings are minimized. These features, along with interdigitation of the ethyl groups, are responsible for its small torsional angles. However, two independent molecules that are present in the asymmetric unit in the triclinic form have very different torsional angles (24.3° for molecule 1 and 15.7° for molecule 2), although the relative ("inward"/"outward") orientation of the ethyl groups within the molecule is exactly same for both molecules. Therefore, the interdigitation of the ethyl groups is not responsible for this large difference (ca. 9°) in the torsional angles observed. There are, however, also no unusually short intermolecular contacts in the crystal packing of the molecule, as seen in Figure 5. Moreover, the average Fe–N_p and Fe–O distances and average out-of-plane displacements (of the 24 porphyrin atoms) are similar in both molecules. However, NSD analysis of the core deformations (Table 4) shows that the cores in molecule 2 have a significant ruffle contribution relative to molecule 1 (and to the molecule in the monoclinic form), which reduces the inter-ring interactions to some extent and is responsible, at least in part, for the lowering of the torsional angle in molecule 2. A similar lowering (6.2°) in the torsional angles is also observed for $[TPPBr_4Fe]_2O$ (Table 5), which crystallizes in two different monoclinic space groups ($P2_1/n$ and $C2/c$) with very similar bond parameters.[18a,18d] However, lowering of the torsional angles is seen for the molecule that has more ruffling ($P2_1/n$), which accommodates the steric congestion at the periphery to some extent.[23]

All the Fe^{III}-oxo-bridged dimers reported here are very stable in both solid and solution phases and do not cleave to form the monomeric species in solution, even in the presence of nitrogenous axial ligands such as pyridines, imidazoles etc. The ^1H NMR spectra of the oxo-bridged dimers in $CDCl_3$ (acid free) at 295 K are very similar. The *meso* proton signals are assigned to the signal at around 6.5 ppm, while the signals for the methylene and methyl protons are in the range 4.3–6.4 ppm and 1.3–1.8 ppm, respectively (see Experimental Section). The shifting of the peaks for the methylene proton by less than 0.5 ppm for $[Fe(tn\text{-}OEP)]_2O$ and $[Fe(trn\text{-}OEP)]_2O$ over the temperature range 20 to –45 °C is also indicative of strong antiferromagnetic coupling between the two iron(III) centers.[17] No EPR signals were observed either in the solid state or in solution (77 K) for the oxo-bridged dimers reported here, which is consistent with large (negative) values of the coupling constant *J*. Variable temperature magnetic susceptibility measurements have been carried out for the crystalline samples of $[Fe(tn\text{-}OEP)]_2O$ between 5 and 350 K. The $\chi_M T$ vs. T data has been subjected to a least-squares fit to the expression[24] derived from the spin Hamiltonian $H = -2JS_1S_2$, where $S_1 = S_2 = 5/2$; the plot of $\chi_M T$ vs. T is shown in Figure 7. The $\chi_M T$ value decreases gradually from 0.63 $cm^3 mol^{-1} K$ at 350 K to a plateau at about 75 K, which is consistent for strongly antiferromagnetically coupled $S = 5/2$ pairs. The residual magnetism observed at low temperature is attributed to paramagnetic impurities, possibly related to the presence of a small amount of mononuclear Fe^{III} impurities. The best fit yields $J = -161$ cm^{-1} with $g = 2.0$ (fixed), $\rho = 1.2\%$ with $R = 5.5 \times 10^{-7}$ [ρ is the molar percentage of mononuclear Fe^{III} ($S = 5/2$) paramagnetic impurities] and confirms the antiferromagnetic nature of the complex. The solution magnetic moment at 295 K for $[Fe(trn\text{-}OEP)]_2O$ and $[Fe(tn\text{-}OEP)]_2O$ in dichloromethane (acid free) calculated by Evan's method[25] is found to be 2.20 and 2.15 BM, respectively, which are also close to the value (2.00 BM) obtained for $[Fe(tn\text{-}OEP)]_2O$ in the crystalline state.

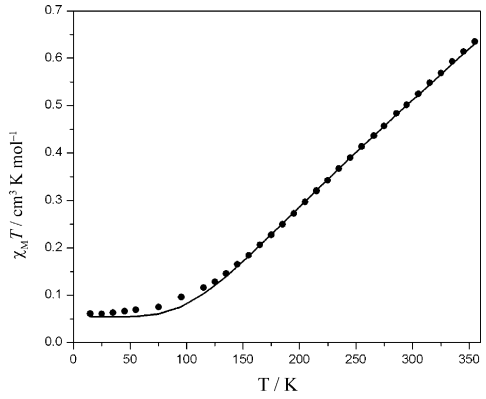

Figure 7. Plot of $\chi_M T$ vs. T for the crystalline samples of [Fe(tn-OEP)]$_2$O. Solid line corresponds to the best fit.

Cyclic Voltammetry

Cyclic voltammetric experiments were done at 25 °C under N_2 in CH_2Cl_2 with 0.1 M tetrabutylammonium hexafluorophosphate (TBAH) as the supporting electrolyte. The electrochemical data are summarized in Table 6, and a representative cyclic voltammogram for [Fe(din-OEP)]$_2$O is shown in Figure S1 (see Supporting Information). The electrochemical data reveal that the complexes undergo two one-electron oxidations and four one-electron reductions. The nitro groups exert a considerable electronic effect in these redox processes, as can be seen from the monotonic increase in the oxidation potentials and decrease in the reduction potentials with increasing nitro substitution. However, the effect is magnified in the case of [Fe(tn-OEP)]$_2$O, which shows an irreversible oxidation at very high positive values at 1.59 V and four irreversible reductions at –0.39, –0.57, –0.87, and 1.01 V. Similar trends in the redox potentials have also been reported for the free ligands and their Zn complexes.[15a] The main features distinguishing [Fe(tn-OEP)]$_2$O from other oxo-bridged dimers in the series are the severe macrocyclic distortion and the presence of four electron-withdrawing nitro groups in the four *meso* positions. Published electrochemical data[26] on a variety of metalloporphyrins suggest that inducing distortion of the macrocycle leads to a greater ease of oxidation, while the addition of the electron-withdrawing groups leads to a more difficult oxidation process, which predominates in this series. Thus, the addition of four NO_2 groups in the porphyrin macrocycle serves both to protect the reactive *meso* position from rapid oxidative attack and also to stabilize both porphyrin and metal against any oxidative degradation during catalysis. [Fe(tn-OEP)]$_2$O therefore ranks amongst the most-effective catalyst in the oxygenation process.

Conclusions

The successive addition of mono-, di-, tri-, and tetranitro substituents at the *meso* positions of octaethylporphyrins has a marked effect on the electronic structures and geometry of the Fe^{III}-μ-oxo dimers. The structures of four such molecules[Fe(din-OEP)]$_2$O,[Fe(trn-OEP)]$_2$O,[Fe(tn-OEP)]$_2$-O (triclinic), and [Fe(tn-OEP)]$_2$O (monoclinic) have been determined by X-ray structure analysis. The tetranitro-substituted complex [Fe(tn-OEP)]$_2$O has the most-distorted porphyrin macrocycle for any Fe^{III}-oxo-bridged dimer ever reported, with a significant increase in the average Fe–N_p and Fe–O distances and in the Fe atom displacement from the mean porphyrin plane. Moreover, the complex represents the first Fe^{III}-μ-oxo dimer with a dodeca-substituted porphyrin macrocycle. The average out-of-plane displacement of the 24 atoms of the porphyrin core increases in the order [Fe(trn-OEP)]$_2$O < [Fe(din-OEP)]$_2$ < [Fe(tn-OEP)]$_2$-O. The effect is magnified in the case of [Fe(tn-OEP)]$_2$O. The rings in [Fe(din-OEP)]$_2$O and [Fe(tn-OEP)]$_2$O undergo saddle-type distortions, while the rings are mostly distorted in a ruffle-type fashion and are more planar in [Fe(trn-OEP)]$_2$O.

The most important structural feature of the molecules is the very different average N_p–Fe–Fe′–N'_p dihedral angles (torsional angle): 18.8° for [Fe(din-OEP)]$_2$O, 0.0° for [Fe(trn-OEP)]$_2$O, 24.2° for [Fe(tn-OEP)]$_2$O (monoclinic), 24.3° and 15.7° for molecules 1 and 2, respectively, of [Fe(tn-OEP)]$_2$O (triclinic). Complex [Fe(trn-OEP)]$_2$O represents the first example of a fully eclipsed ring orientation for Fe^{III}-μ-oxo porphyrin dimers reported so far. As the number of nitro groups increases, the torsional angles also increases from [Fe(OEP)]$_2$O, to [Fe(din-OEP)]$_2$O, and to [Fe(tn-OEP)]$_2$O. This feature and the pronounced increasing nonplanarity of the porphyrin core arise from the significant steric congestion in the periphery of the molecule. However, rings in [Fe(trn-OEP)]$_2$O are distorted in a ruffle-type fashion and are more planar, and the three nitro groups are placed at the opposite faces of the two rings, which leads to a fully eclipsed ring orientation in order to minimize the intra- and inter-ring interactions.

Table 6. Electrochemical data.[a]

Complex	Oxidation $E_{1/2}(1)$	$E_{1/2}(2)$	Reduction $E_{1/2}(1)$	$E_{1/2}(2)$	$E_{1/2}(3)$	$E_{1/2}(4)$
[Fe(mn-OEP)]$_2$O	1.11(55)[b]	1.36(65)[b]	–0.83[d]	–1.08[d]	–1.32[d]	–1.68[d]
[Fe(dn-OEP)]$_2$O	1.13(70)[b]	1.37(65)[b]	–0.82[d]	–1.06[d]	–1.30[d]	–1.66[d]
[Fe(trn-OEP)]$_2$O	1.17(80)[b]	1.38(90)[b]	–0.69[d,e]	–	–0.91[d]	–1.13[d]
[Fe(tn-OEP)]$_2$O	1.59[c]	–	–0.39[d]	–0.57[d]	–0.87[d]	–1.01[d]

[a] Cyclic voltammogram in CH_2Cl_2. The supporting electrolyte was 0.10 M tetrabutylammonium hexafluorophosphate and the reference electrode was Ag/AgCl. [b] Half-wave potentials $E_{1/2} = (E_{pa} + E_{pc})/2$ (peak potential differences in mV written in parentheses). [c] Irreversible oxidation processes, E_{pa}. [d] Irreversible reduction processes, E_{pc}. [e] Two-electron reduction processes.

The two independent molecules that are present in the asymmetric unit of [Fe(tn-OEP)]$_2$O (triclinic) have very different torsional angles. However, the cores in molecule 2 have a significant ruffle contribution relative to molecule 1, which reduces the inter-ring interactions and is responsible for the lowering of the torsional angle in molecule 2. Our study suggests that ruffling of the porphyrin macrocycle accommodates the steric congestion at the periphery in Fe^{III}-μ-oxo porphyrin dimers, which leads to lower torsional angles.

All the oxo-bridged dimers reported here are very stable in both solid and solution phases. Spectroscopic studies are indicative of strong antiferromagnetic coupling between the two high-spin iron(III) centers. Electrochemical data obtained from cyclic voltammetric studies reveal that the complexes are easier to reduce but become more difficult to oxidize with progressive addition of nitro groups to the *meso* positions, and the effect is magnified in the case of [Fe(tn-OEP)]$_2$O. Thus, the addition of four NO_2 groups in the porphyrin macrocycle serves both to protect the reactive *meso* position from rapid oxidative attack and also to stabilize both the porphyrin and metal against any oxidative degradation during catalysis. As a result, [Fe(tn-OEP)]$_2$O ranks amongst the most-effective catalyst in the oxygenation process.

Experimental Section

Materials: Reagents and solvents were purchased from commercial sources and purified by standard procedures before use. Grade I neutral alumina was used for column chromatography. H_2OEP,[27] 5-mononitrooctaethylporphyrin (mn-H_2OEP),[14] 5,10-dinitrooctaethylporphyrin (din-H_2OEP),[14] 5,10,15-trnitrooctaethylporphyrin (trn-H_2OEP),[14] and tetranitrooctaethylporphyrin (tn-H_2OEP)[15] were prepared by literature methods. Iron was inserted by a standard procedure[16] under a dioxygen-free, dinitrogen atmosphere, which produced the corresponding Fe(por)Cl in excellent yields.

Synthesis: The Fe^{III}-μ-oxo dimers were prepared using a general method. Details are given below for a representative case.

Preparation of [Fe(din-OEP)]$_2$O: Fe(din-OEP)Cl (100 mg, 0.14 mmol) was dissolved in dichloromethane (100 mL) and stirred for 5 min. Sodium hydroxide (100 mL of a 2 M aqueous solution) was added to the mixture and stirred for 1 h. The organic layer was separated, which was then washed with water until free from NaOH and dried with anhydrous Na_2SO_4. The solvents from the resulting solution were evaporated to dryness, and the product was purified by column chromatography by using basic alumina. The major green fraction eluted with dichloromethane was collected and vacuum dried to give a reddish green solid of the complex. Yield: 135 mg, 70%. $C_{72}H_{84}N_{12}O_9Fe_2$ (1372.52): calcd. C 63.03, H 6.16, N 12.24; found C 63.02, H 6.14, N 12.22. UV/Vis (chloroform): λ_{max} (ε, $M^{-1}cm^{-1}$) = 378 (2.95×10^4), 563 (4.29×10^3), 595 (3.4×10^3) nm. IR (KBr): $\tilde{\nu}$ = 1371, 1530 (N–O stretch), 875 (Fe–O–Fe stretch) cm^{-1}. ^{1}H NMR (500 MHz, $CDCl_3$, 295 K): δ = 6.48 (s, 2 H, *meso* C–H), 4.31, 4.41, 5.02, 5.06, 5.26, 5.35, 5.85, 6.00 (br., 16 H,–CH_2–), 1.29, 1.49, 1.58, 1.78 (br., 24 H,–CH_3) ppm.

The following compounds were prepared using similar procedures.

[Fe(mn-OEP)]$_2$O: Yield: 75%. $C_{72}H_{86}Fe_2N_{10}O_5$ (1282.56): calcd. C 67.43, H 6.75, N 10.92; found C 67.48, H 6.78, N 10.94. UV/Vis (chloroform): λ_{max}, (ε, $M^{-1}cm^{-1}$) = 380 (2.73×10^4), 562 (4.32×10^3), 594 (3.34×10^3) nm. IR (KBr): 1374, 1528 (N–O stretch), 878 (Fe–O–Fe stretch) cm^{-1}. ^{1}H NMR (500 MHz, $CDCl_3$, 295 K): δ = 6.50 (s, 1 H, *meso* C–H), 6.40 (s, 2 H, *meso* C–H), 4.32, 4.42, 5.06, 5.26, 5.35, 5.78, 6.02, 6.41 (br., 16 H, –CH_2–), 1.28, 1.50, 1.56, 1.77 (br., 24 H, –CH_3) ppm.

[Fe(trn-OEP)]$_2$O: Yield: 60%. $C_{72}H_{82}Fe_2N_{14}O_{13}$ (1462.49): calcd. C 59.13, H 5.65, N 13.40; found C 59.20, H 5.62, N 13.42. UV/Vis (chloroform): λ_{max}, (ε, $M^{-1}cm^{-1}$) 361 (2.76×10^4), 566 (4.12×10^3), 596 (2.98×10^3) nm. IR (KBr): 1364, 1533 (N–O stretch), 866 (Fe–O–Fe stretch) cm^{-1}. ^{1}H NMR (500 MHz, $CDCl_3$, 295 K): δ = 6.60 (s, 1 H, *meso* C–H), 4.40, 4.56, 5.24, 5.39, 5.71, 6.10, 6.20, 6.40 (br., 16 H, –CH_2–), 1.48, 1.62, 1.64, 1.83 (br., 24 H, –CH_3) ppm.

[Fe(tn-OEP)]$_2$O: Yield: 70%. $C_{72}H_{80}Fe_2N_{16}O_{17}$ (1552.46): calcd. C 55.70, H 5.19, N 14.43; found C 55.65, H 5.16, N 14.41. UV/Vis (chloroform): λ_{max}, (ε, $M^{-1}cm^{-1}$) 369 (2.85×10^4), 577 (3.89×10^3), 612 (2.5×10^3) nm. IR (KBr): 1365, 1535 (N–O stretch), 849 (Fe–O–Fe stretch) cm^{-1}. ^{1}H NMR (500 MHz, $CDCl_3$, 295 K): δ = 4.50, 5.80 (br., 16 H, –CH_2–), 1.36 (br., 24 H, –CH_3) ppm.

Instrumentation: UV/Vis spectra were recorded on a PerkinElmer UV/Vis spectrometer. Elemental (C, H, and N) analyses were performed on a Perkin–Elmer 2400II elemental analyzer. Electron paramagnetic resonance (EPR) spectra were obtained with a Bruker EMX EPR spectrometer. Magnetic susceptibility data were collected by using a Quantum Design MPMS SQUID magnetometer over the temperature range 5–350 K. Data were collected in applied fields of 1 T and corrected for diamagnetism with Pascal's constants. ^{1}H NMR spectra were recorded on a JEOL 500 MHz instrument. Cyclic voltammetric studies were performed on a BAS Epsilon electrochemical workstation in dichloromethane with 0.1 M tetrabutylammonium hexafluorophosphate (TBAH) as supporting electrolyte. The working electrode was a BAS glassy carbon disk electrode with a 3-mm radius, the reference electrode was Ag/AgCl, and the auxiliary electrode was Pt wire. The concentration of the compounds was in the order of 10^{-3} M. The ferrocene/ferrocenium couple occurs at $E_{1/2}$ = +0.45(65) V vs. Ag/AgCl under the same experimental conditions.

Structure Solution and Refinement: The crystals were coated with light hydrocarbon oil and mounted onto a Bruker SMART APEX CCD diffractometer equipped with CRYO Industries low-temperature apparatus, under a dinitrogen stream at 100 K ([Fe(trn-OEP)]$_2$O at 295 K), and intensity data were collected by using graphite-monochromated Mo-K_α radiation (λ = 0.71073 Å). The data integration and reduction were processed with the SAINT[28] software. An absorption correction was applied.[29] Structures were solved by the direct method with SHELXS-97 and were refined on F^2 by full-matrix least-squares with the SHELXL-97[30] program package. Non-hydrogen atoms were refined anisotropically. Hydrogen atoms were included in geometrically calculated positions and were refined according to the "riding model". The "SQUEEZE" option in PLATON[31] was used to remove a disordered solvent molecule from the overall intensity data of the compounds [Fe(trn-OEP)]$_2$O and [Fe(tn-OEP)]$_2$O (monoclinic form)]. Crystal data are given in Table 7. CCDC-694073, -694071, -694074, and -694072 for [Fe(din-OEP)]$_2$O, [Fe(trn-OEP)]$_2$O, [Fe(tn-OEP)]$_2$O [Tric.], and [Fe(tn-OEP)]$_2$O [Mono.], respectively, contain the supplementary crystallographic data for this paper. These data can be obtained free of charge from the Cambridge Crystallographic Data Centre via www.ccdc.cam.ac.uk/data_request/cif.

Table 7. Crystal data and data collection parameters.

	[Fe(din-OEP)]$_2$O	[Fe(trn-OEP)]$_2$O	[Fe(tn-OEP)]$_2$O	[Fe(tn-OEP)]$_2$O·EtOH·0.5H$_2$O·0.5CHCl$_3$·0.33C$_6$H$_{12}$
T [K]	100(2)	295(2)	100(2)	100(2)
*F*ormula	$C_{146}H_{171}Fe_4N_{25}O_{18}$	$C_{72}H_{82}Fe_2N_{14}O_{13}$	$C_{72}H_{80}Fe_2N_{16}O_{17}$	$C_{76.48}H_{91.46}C_{1.50}Fe_2N_{16}O_{18.5}$
*F*ormula weight	2787.48	1463.22	1553.22	1695.75
Color and Habit	dark brown	dark brown	dark brown	dark brown
Crystal system	monoclinic	triclinic	triclinic	monoclinic
Space group	$P2(1)/n$	$P\bar{1}$	$P\bar{1}$	$P2(1)/n$
a [Å]	16.4912(11)	10.975(5)	14.0583(10)	11.4771(9)
b [Å]	16.1049(10)	13.985(7)	19.8631(14)	26.419(2)
c [Å]	27.3169(18)	14.846(7)	26.3823(18)	27.421(2)
α [°]	90	110.177(8)	102.3070(10)	90
β [°]	98.2350(10)	108.432(7)	92.9710(10)	95.693(2)
γ [°]	90	99.018(9)	92.4100(10)	90
V [Å^3]	7180.3(8)	1936.6(16)	7177.4(9)	8273.5(12)
Radiation (λ [Å])	Mo-K_α (0.71073)	Mo-K_α (0.71073)	Mo-K_α (0.71073)	Mo-K_α (0.71073)
Z	2	1	4	4
$d_{calcd.}$ [g cm^{-3}]	1.289	1.255	1.437	1.361
μ [mm^{-1}]	0.469	0.442	0.486	0.476
$F(000)$	2940	768	3248	3551
No. unique data	13317	6871	26134	16200
No. restraints	5	0	2	0
No. parameters refined	961	465	2010	983
GOF on F^2	1.037	1.030	1.055	0.903
R_1[a]	0.0826	0.0635	0.0648	0.0635
wR_2[b]	0.2526	0.1649	0.1474	0.1705

[a] *F*or data with $I > 2\sigma I$; $R_1 = [\Sigma||F_o| - |F_c||]/\Sigma|F_o|$. [b] *F*or all data; $wR_2 = \{\Sigma[w(F_o^2 - F_c^2)^2]/\Sigma[w(F_o^2)^2]\}^{1/2}$.

Supporting Information (see footnote on the first page of this article): X-ray structure refinement details for [Fe(din-OEP)]$_2$O, [Fe(trn-OEP)]$_2$O, [Fe(tn-OEP)]$_2$O [Tric.], and [Fe(tn-OEP)]$_2$O [Mono.] and a representative cyclic voltammogram for [Fe(din-OEP)]$_2$O are presented.

Acknowledgments

We are thankful to the Department of Science and Technology, New Delhi, and the Council of Scientific and Industrial Research, New Delhi for financial support. The authors also thank Mr. Sukanta Mandal for the least-squares fit of the magnetic data.

[1] a) J. A. Shelnutt in *The Porphyrin Handbook* (Eds.: K. M. Kadish, K. M. Smith, R. Guilard), Academic Press, New York, **2000**, vol. 7, p. 167–223; b) J. A. Shelnutt, X.-Z. Song, J.-G. Ma, S.-L. Jia, W. Jentzen, C. J. Medforth, *Chem. Soc. Rev.* **1998**, *27*, 31–42.

[2] a) M. O. Senge in *The Porphyrin Handbook* (Eds.: K. M. Kadish, K. M. Smith, R. Guilard), Academic Press, New York, **2000**, vol. 1, p. 239–347; b) M. O. Senge, *Chem. Commun.* **2006**, 243–256; c) M. Ravikanth, T. K. Chandrashekar, *Structure and Bonding, Vol. 82*, Springer, Berlin, **1995**, p. 105–188.

[3] a) M. Nakamura, Y. Ohgo, A. Ikezaki, *J. Inorg. Biochem.* **2008**, *102*, 433–445; b) M. Nakamura, *Coord. Chem. Rev.* **2006**, *250*, 2271–2294; c) F. A. Walker, *Chem. Rev.* **2004**, *104*, 589–615; d) F. A. Walker, *Coord. Chem. Rev.* **1999**, *185–186*, 471–534.

[4] a) W. R. Scheidt in *The Porphyrin Handbook* (Eds.: K. M. Kadish, K. M. Smith, R. Guilard), Academic Press, New York, **2000**, vol. 3, p. 49–112; b) W. R. Scheidt, C. A. Reed, *Chem. Rev.* **1981**, *81*, 543–555.

[5] a) S. K. Ghosh, R. Patra, S. P. Rath, *Inorg. Chem.* **2008**, *47*, 9848–9856; b) R. Patra, A. Chaudhury, S. K. Ghosh, S. P. Rath, *Inorg. Chem.* **2008**, *47*, 8324–8335; c) K. M. Barkigia, M. W. Renner, M. O. Senge, J. Fajer, *J. Phys. Chem. B* **2004**, *108*, 2173–2180; d) M. O. Senge, *J. Porphyrins Phthalocyanines* **1998**, *2*, 107–121; e) M. O. Senge, K. M. Smith, *J. Chem. Soc., Chem. Commun.* **1994**, 923–924.

[6] a) *The Activation of Dioxygen and Homogeneous Catalytic Oxidation* (Eds.: D. H. R. Barton, A. E. Martell, D. T. Sawyer), Plenum Press, New York, **1993**; b) R. A. Shelton (Ed.), *Metalloporphyrins in Catalytic Oxidations*, Marcel Dekker, Inc., New York, **1994**.

[7] a) M. W. Grinstaff, M. G. Hill, J. A. Labinger, H. B. Gray, *Science* **1994**, *264*, 1311–1313; b) P. E. Ellis, J. E. Lyons, *Coord. Chem. Rev.* **1990**, *105*, 181–193; c) K. M. Barkigia, M. Palacio, Y. Sun, M. Nogues, M. W. Renner, F. Varret, P. Battioni, D. Mansuy, J. Fajer, *Inorg. Chem.* **2002**, *41*, 5647–5649; d) K. T. Moore, I. T. Horváth, M. J. Therien, *Inorg. Chem.* **2000**, *39*, 3125–3139; e) K. T. Moore, J. T. Fletcher, M. J. Therien, *J. Am. Chem. Soc.* **1999**, *121*, 5196–5209; f) M. W. Grinstaff, M. G. Hill, E. R. Birnbaum, W. P. Schaefer, J. A. Labinger, H. B. Gray, *Inorg. Chem.* **1995**, *34*, 4896–4902; g) T. Wijesekera, A. Matsumoto, D. Dolphin, D. Lexa, *Angew. Chem. Int. Ed. Engl.* **1990**, *29*, 1028–1030; h) C. K. Chang, K. M. Barkigia, L. K. Hanson, J. Fajer, *J. Am. Chem. Soc.* **1986**, *108*, 1352–1354.

[8] a) B. Meunier, S. P. de Visser, S. Shaik, *Chem. Rev.* **2004**, *104*, 3947–3980; b) J. T. Groves, K. Shalyaev, J. Lee in *The Porphyrin Handbook* (Eds.: K. M. Kadish, K. M. Smith, R. Guilard), Academic Press, New York, **2000**, vol. 4, p. 17–40; c) B. Meunier, A. Robert, G. Pratviel, J. Bernadou in *The Porphyrin Handbook* (Eds.: K. M. Kadish, K. M. Smith, R. Guilard), Academic Press, New York, **2000**, vol. 4, p. 119–187.

[9] a) P. D. Harvey, C. Stern, C. P. Gros, R. Guilard, *Coord. Chem. Rev.* **2007**, *251*, 401–428; b) J. Rosenthal, J. Bachman, J. L. Dempsey, A. J. Esswein, T. G. Gray, J. M. Hodgkiss, D. R. Manke, T. D. Luckett, B. J. Pistorio, A. S. Veige, D. G. Nocera, *Coord. Chem. Rev.* **2005**, *249*, 1316–1326; c) J. Rosenthal, T. D. Luckett, J. M. Hodgkiss, D. G. Nocera, *J. Am. Chem. Soc.* **2006**, *128*, 6546–6547; d) J. Rosenthal, B. J. Pistorio, L. L. Chng, D. G. Nocera, *J. Org. Chem.* **2005**, *70*, 1885–1888.

[10] a) W.-D. Woggon, *Acc. Chem. Res.* **2005**, *38*, 127–136; b) I. G. Denisov, T. M. Makris, S. G. Sligar, I. Schlichting, *Chem. Rev.* **2005**, *105*, 2253–2277; c) P. Ortiz de Montellano, *Cytochrome*

P-450: Structure, Mechanism and Biochemistry, Plenum, New York, **1986**.
[11] a) W. P. Schaefer, P. E. Ellis, J. E. Lyons, S. N. Shaikh, *Acta Crystallogr., Sect. C* **1995**, *51*, 2252–2255; b) P. E. Ellis Jr, J. E. Lyons, S. N. Shaikh, *Catal. Lett.* **1994**, *24*, 79–83; c) C.-C. Guo, *J. Catal.* **1998**, *178*, 182–187.
[12] R. B. Woodward, *Angew. Chem.* **1960**, *72*, 651–662.
[13] B. Cheng, J. D. Hobbs, P. G. Debrunner, J. Erlebacher, J. A. Shelnutt, W. R. Scheidt, *Inorg. Chem.* **1995**, *34*, 102–110.
[14] R. Bonnett, G. F. Stephenson, *J. Org. Chem.* **1965**, *30*, 2791–2798.
[15] a) L. Gong, D. Dolphin, *Can. J. Chem.* **1985**, *63*, 401–405; b) L. Gong, D. Dolphin, *Can. J. Chem.* **1985**, *63*, 406–411.
[16] A. D. Adler, F. R. Lango, F. Kampas, *J. Inorg. Nucl. Chem.* **1970**, *32*, 2443–2445.
[17] W. R. Scheidt, B. Cheng, M. K. Safo, F. Cukiernik, J.-C. Marchon, P. G. Debrunner, *J. Am. Chem. Soc.* **1992**, *114*, 4420–4421.
[18] a) M. Li, M. Shang, H. F. Duval, W. R. Scheidt, *Acta Crystallography. Sect. C: Cryst. Struct. Commun.* **2000**, *56*, 1206–1207; b) A. R. Li, H. H. Wei, L. L. Gang, *Inorg. Chim. Acta* **1999**, *290*, 51–56; c) X. D. Jiao, J. W. Huang, L. N. Ji, B. S. Luo, L. R. Chen, *J. Inorg. Biochem.* **1997**, *65*, 229–233; d) K. M. Kadish, M. Antret, Z. Ou, P. Tagliatesta, T. Boschi, V. Fares, *Inorg. Chem.* **1997**, *36*, 204–207; e) T. J. Bartczak, L. Latos-Grazynski, A. Wyslouch, *Inorg. Chim. Acta* **1990**, *171*, 205–212; f) S. H. Strauss, M. J. Pawlik, J. Skowyra, J. R. Kennedy, O. P. Anderson, K. Spartalian, J. L. Dye, *Inorg. Chem.* **1987**, *26*, 724–730; g) K. L. Lay, J. W. Buchler, J. E. Kenny, W. R. Scheidt, *Inorg. Chim. Acta* **1986**, *123*, 91–97.
[19] a) S. K. Ghosh, R. Patra, S. P. Rath, *Inorg. Chem.* **2008**, *47*, 10196–10198; b) H. M. Lee, M. M. Olmstead, G. G. Gross, A. L. Balch, *Cryst. Growth Des.* **2003**, *3*, 691–697; c) M. A. Ivanca, A. G. Lappin, W. R. Scheidt, *Inorg. Chem.* **1991**, *30*, 711–718; d) A. Gold, K. Jayaraj, P. Doppelit, J. Fischer, R. Weiss, *Inorg. Chim. Acta* **1988**, *150*, 177–181; e) P. N. Swepston, J. A. Ibera, *Acta Crystallogr., Sect. C* **1985**, *41*, 671–673; f) J. T. Landrum, D. Grimmett, K. J. Haller, W. R. Scheidt, C. A. Reed, *J. Am. Chem. Soc.* **1981**, *103*, 2640–2650; g) A. B. Hoffman, D. M. Collins, V. W. Day, E. B. Fleischer, T. S. Srivastava, J. L. Hoard, *J. Am. Chem. Soc.* **1972**, *94*, 3620–3626.
[20] W. R. Scheidt, Y. J. Lee, *Struct. Bonding (Berlin)* **1987**, *64*, 1–70.
[21] a) W. Jentzen, J.-G. Ma, J. A. Shelnutt, *Biophys. J.* **1998**, *74*, 753–763; b) W. Jentzen, X.-Z. Song, J. A. Shelnutt, *J. Phys. Chem. B* **1997**, *101*, 1684–1699.
[22] L. Sun, W. Jentzen, J. A. Shelnutt, *The Normal Coordinate Structural Decomposition Engine*; http://jasheln.unm.edu/jasheln/content/nsd/NSDengine.
[23] NSD[21,22] analysis of the porphyrin ring deformations for $[TPPBr_4Fe]_2O$ obtained from two X-ray crystal data sets[18a,18d] shows significant ruffle contributions of 28.7% for the molecule that crystallizes in the *C*2/*c* space group and 32.3 (core I) and 32.8% (core II) for the molecule that crystallizes in the $P2_1/n$ space group.
[24] C. J. O'Connor, *Prog. Inorg. Chem.* **1982**, *29*, 203.
[25] D. F. Evans, *J. Chem. Soc.* **1959**, 2003.
[26] K. M. Kadish, E. V. Caemelbecke, G. Royal in *The Porphyrin Handbook* (Eds.: K. M. Kadish, K. M. Smith, R. Guilard), Academic Press, New York, **2000**, vol 8, p. 1–97.
[27] L. J. Sessler, A. Mozaffari, M. R. Johnson, *Org. Synth.* **1992**, *70*, 68–78.
[28] *SAINT+*, 6.02 ed., Bruker AXS, Madison, WI, **1999**.
[29] G. M. Sheldrick, *SADABS*, **2007**.
[30] G. M. Sheldrick, *Acta Crystallogr., Sect. A* **2008**, *64*, 112–122.
[31] A. L. Spek, *PLATON-A Multipurpose Crystallographic Tool*, University of Utrecht, Utrecht, The Netherlands, **2003**.

Received: August 10, 2008
Published Online: January 14, 2009

